Effect of Sediments on Aqueous Silica Transport in Subduction Zones

Craig E. Manning

Department of Earth and Space Sciences, University of California, Los Angeles, California

Where sediments are present at the slab-mantle interface in subduction zones, most migration paths of aqueous solutions will result in chemical interaction between sediment and fluid. The ability of sediment to influence fluid composition can be appreciated by examining aqueous Si concentrations with a model chemical system, K_2O-Al_2O_3-SiO_2-H_2O, for three subduction-zone pressure-temperature trajectories (*PT* paths). Analysis of mineral-melt-H_2O phase relations as a function of aqueous Si concentration shows that metasedimentary mineral assemblages fix dissolved silica contents at or near those required by quartz saturation, even in the absence of quartz. Changes in dissolved silica content with pressure and temperature are much greater than those required by the range in plausible mineral assemblages. Sediments thus influence Si transport in subduction zones by buffering fluids at the slab-mantle interface at or near quartz saturation as pressure and temperature change, and, as a result, maximizing aqueous Si concentrations along the slab-mantle interface. Changes in pressure and temperature along model slab trajectories result in increases in Si content of pore fluids by ~10^3 and ~10^5 times along the lowest and highest temperature paths, respectively. The spatial gradient in dissolved silica concentration also increases with depth, and is greater for higher temperature *PT* paths. Most Si redistribution will occur in the deep portions of high-temperature subduction zones, and fluid-sediment interaction dictates that the amount of aqueous silica transported from the slab to the mantle wedge at any point along the slab-mantle interface is maximized if equilibrium is attained.

1. INTRODUCTION

Subduction zones can be divided into those that accumulate, or accrete, sediments, and those that do not [*von Heune and Scholl*, 1991]. In non-accreting margins, all ocean-floor sediment transported to the trench is subducted; in accreting margins, a décollement develops in the sedimentary section, below which all material transported to the trench is subducted. The décollement most likely develops near the interface between ocean-floor sediments and the overlying clastic wedge [*Moore*, 1975; *Plank*, 1993; *Plank and Langmuir*, 1993]. Downgoing slabs are therefore mantled by a veneer of ocean-floor sediments, which may be hundreds of meters thick [*Plank and Langmuir*, 1993].

Subduction: Top to Bottom
Geophysical Monograph 96

Studies of volcanic arcs and subduction complexes suggest that sediments exert an important control on the petrology, magmatic evolution, and aqueous geochemistry of convergent margins [e.g., *Church*, 1976; *Kay et al.*, 1978; *Sun*, 1980; *Whitford and Jezek*, 1982; *White and Dupré*, 1986; *Tera et al.*, 1986; *Morris et al.*, 1990; *Ernst*, 1990; *Peacock*, 1990; *Bebout and Barton*, 1993; *Philippot*, 1993; *Plank and Langmuir*, 1993]. The physical and chemical mechanisms by which sediments influence subduction processes remain poorly understood, but redistribution of chemical components by aqueous fluids provides a viable hypothesis for material transport in this environment [e.g., *Tatsumi*, 1989; *Bebout and Barton*, 1989, 1993; *Bebout*, 1991; *Davies and Stevenson*, 1992]. As illustrated in Figure 1, sediments may mix mechanically with mantle material along the slab-mantle interface, or with other components of the subducting lithosphere. Fluids will be liberated by metamorphic devolatilization reactions in either sediments or mafic and ultramafic portions of the subducting plate. Wide variations in possible pressure and temperature gradi-

ents in subduction zones, coupled with strongly heterogeneous permeability-fields, imply that low-density fluids may have flux vectors with directions ranging from subvertical to updip along the slab. Figure 1 shows that of the potential flux directions, only fluids liberated in, and remaining in, oceanic basement rocks will not interact with sediments. In cases where the slab melts, movement of the resulting magma into the mantle wedge will also require chemical interaction with subducted sedimentary material.

Recent studies have addressed the role played by sediments in the redistribution of chemical components by aqueous fluids during subduction [*Bebout and Barton*, 1989, 1993; *Ernst*, 1990; *Peacock*, 1990; *Bebout*, 1991]. As noted by *Bebout and Barton* [1993], such studies are hindered by the lack of experimental data or theoretical models for mineral solubility at subduction-zone conditions. However, new experimental developments now allow the acquisition of these data [*Ayers and Watson*, 1991, 1993; *Brenan and Watson*, 1991; *Brenan*, 1993; *Manning*, 1994, *Manning and Boettcher*, 1994], which can be incorporated into coupled reaction and fluid-flow models of subducting slabs and the mantle wedge [e.g., *Manning*, 1995]. I have combined this approach with phase equilibrium calculations in the model system K_2O-Al_2O_3-SiO_2-H_2O (KASH) to illustrate how sediment may control the concentration and transport potential of a major element, silicon, in subduction zones.

2. METHODS

As a model for sediment-fluid interaction, I evaluated phase relations in the KASH system assuming the presence of an Al or Al-Si mineral and H_2O. This provides an approximation of subducting Al-rich pelagic sediment, which is dominated by micas, aluminosilicate clays, and quartz, and allows illustration of the first-order consequences of subduction of this sediment on element transport by aqueous solutions.

Analysis of phase relations in a model system is a simplification limiting the bulk compositions addressed by the calculations. For example, subducting sedimentary material may be a mixture of pelagic, terrigenous, and arc-derived sediment [e.g., *von Heune and Scholl*, 1991]; such sediments would be better approximated in the KASH system by assuming the presence of K feldspar instead of an Al or Al-Si mineral. In addition, this analysis ignores biogenic carbonate, which could lead to significant dissolved carbon species. This is reasonable for modern subduction, in which little biogenic carbonate is consumed [e.g., *Plank*, 1993]; but it limits applicability to subduction environments rich in CO_2. Finally, pelagic sediments range widely in composition [e.g., *Kyte et al.*, 1993; *Plank and Ludden*, 1992; *Plank and Langmuir*, 1993]. Important components not considered here include Na and Mg. On average, pelagic sediments have subequal molar concentrations of Na and K, and increasing Mg leads to the formation of chlorite, smectite, and/or phengite rather than aluminosilicate clays and muscovite. Model KASH sediment therefore corresponds to an aluminous, potassic, Mg-poor end member of the spectrum of pelagic sediment compositions. Similar analyses of phase relations in Mg- and Na-bearing model systems (C. E. Manning, unpublished data) shows that varying chemical components does not significantly alter conclusions about Si dissolution, transport, and precipitation.

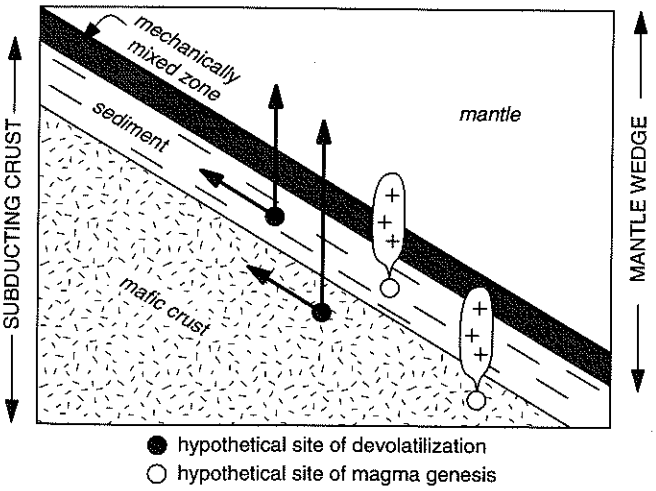

Fig. 1. Schematic illustration of the effect of sediment on material transport in subduction zones. Bold arrows are schematic H_2O flux vectors; crosses denote magma. The only transport path that does not involve interaction with sediment is aqueous fluid liberated from mafic crust and migrating updip within its source. This conceptual model is based on *Bebout and Barton* [1989, 1993] and *Bebout* [1991].

Phase relations were computed for three model subduction zones from *Peacock* [1993]. The steady-state increase in pressure and temperature at the slab-mantle interface with depth in the subduction zone, or *PT* path, was calculated for subduction at 10 cm yr^{-1} at an angle of 20° for rock densities of 3000 kg m^{-3} (Figure 2). The three *PT* paths are distinct in that temperature at a given depth from 0 to ~70 km decreases from Path 1 through Path 3. They can be viewed as illustrating the range in pressure and temperature conditions resulting from different subduction scenarios. For example, Path 1 represents the *PT* regime to be expected when young oceanic crust is subducted, whereas

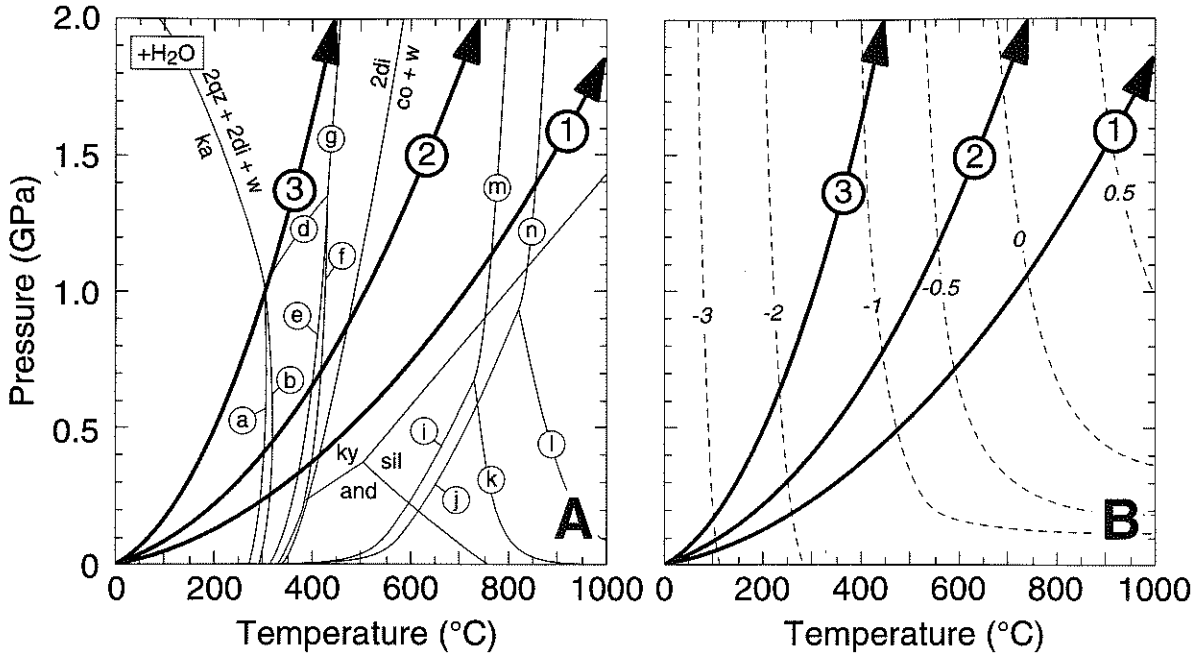

Fig. 2. Pressure-temperature diagrams with *PT* paths 1-3 (bold arrows) from *Peacock* [1993] (see text). (A) Phase relations in the system K_2O-Al_2O_3-SiO_2-H_2O and in the presence of H_2O. All phases assumed to be stoichiometric, with unit activity. Mineral-H_2O equilibria calculated using *Berman* [1988 (1992 extension)] and *Haar et al.* [1984]; mineral-melt-H_2O equilibria are from *Storre and Karotke* [1972] and *Huang and Wyllie* [1974]. Abbreviations: and, andalusite; co, corundum; di, diaspore; ka, kaolinite; ky, kyanite; qz, quartz; sil, sillimanite; w, water. Reaction boundaries labeled with circled letters keyed to Table 1. (B) Isopleths of $\log m_{SiO2(aq)}$ calculated using the equation of *Manning* [1994].

Path 3 probably best reflects conditions likely in a long-lived, steady state subduction zone. Although different, more complex *PT* paths may result from consideration of the brittle-ductile transition [*Peacock et al.*, 1994] or alternative numerical analyses of heat and mass transfer [e.g., *Davies and Stevenson*, 1992], the paths used here serve as a simple framework to illustrate how changes in pressure and temperature influence aqueous mass transfer of Si from the Earth's surface to 2 GPa.

3. PHASE RELATIONS IN THE MODEL SEDIMENT

Figure 2a shows equilibria relevant to high pressure metamorphism and melting in the KASH system, with the *PT* paths of the three subduction zones. Equilibria in Figure 2a are listed in Table 1. Not shown for simplicity are the α–β quartz transition, low-pressure high-temperature equilibria involving leucite and melt, and low-pressure low-temperature reactions involving silica and clay diagenesis.

Each path traverses different regions of the *P T* projection, which results in contrasting phase relations. Along Path 1, dehydration of hydrous Al and Al-Si minerals occurs at low pressures in the upper levels of the subduction zone, such that muscovite + kyanite will be the stable mineral assemblage in the presence of quartz and H_2O from ~0.4-1.1 GPa (14-37 km depth). Below this point, a KASH melt forms (equilibrium *m*, Table 1). Note that the assumption of the presence of an aluminosilicate mineral prevents the stable existence of K feldspar with muscovite at high pressures, which leads to the water-saturated solidus geometry defined by equilibria *k* and *m* (Figure 2a, Table 1). Melting in the presence of K feldspar instead of kyanite would produce the more familiar solidus geometry and would occur at 32 km, which is 5 km shallower, or 15 km updip, of the melting position in Figure 2a. Neither case corresponds to the temperature of melting of natural pelagic clay in the presence of H_2O (~650°C, *Nichols et al.* [1994]); but, despite this discrepancy, the effect of melt on metasomatic phase relations can still be evaluated from the equilibria in Figure 2a (see below).

Along Path 2, the maximum depth of dehydration of hydrous Al and Al-Si minerals (equilibria *e, f,* and *h*, Table 1)

TABLE 1. Relevant Equilibria in the KASH System

$$Al_2Si_2O_5(OH)_4 + 2SiO_2 = Al_2Si_4O_{10}(OH)_2 + H_2O \quad (a)$$
kaolinite quartz pyrophyllite

$$2Al_2Si_2O_5(OH)_4 = 2AlOOH + Al_2Si_4O_{10}(OH)_2 + 2H_2O \quad (b)$$
kaolinite diaspore pyrophyllite

$$Al_2Si_2O_5(OH)_4 = 2SiO_2 + 2AlOOH + H_2O \quad (c)$$
kaolinite quartz diaspore

$$2AlOOH + 4SiO_2 = Al_2Si_4O_{10}(OH)_2 \quad (d)$$
diaspore quartz pyrophyllite

$$6AlOOH + Al_2Si_4O_{10}(OH)_2 = 4Al_2SiO_5 + 4H_2O \quad (e)$$
diaspore pyrophyllite

$$Al_2Si_4O_{10}(OH)_2 = 3SiO_2 + Al_2SiO_5 + H_2O \quad (f)$$
pyrophyllite quartz

$$2AlOOH + SiO_2 = Al_2SiO_5 + H_2O \quad (g)$$
diaspore quartz

$$2AlOOH = Al_2O_3 + H_2O \quad (h)$$
diaspore corundum

$$KAl_3Si_3O_{10}(OH)_2 + SiO_2 = KAlSi_3O_8 + Al_2SiO_5 + H_2O \quad (i)$$
muscovite quartz K feldspar

$$KAl_3Si_3O_{10}(OH)_2 = KAlSi_3O_8 + Al_2O_3 + H_2O \quad (j)$$
muscovite K feldspar corundum

$$KAlSi_3O_8 + Al_2SiO_5 + SiO_2 + H_2O = \text{Melt} \quad (k)$$
K feldspar quartz

$$KAlSi_3O_8 + Al_2O_3 + H_2O = \text{Melt} \quad (l)$$
K feldspar corundum

$$KAl_3Si_3O_{10}(OH)_2 + SiO_2 + H_2O = Al_2SiO_5 + \text{Melt} \quad (m)$$
muscovite quartz

$$KAl_3Si_3O_{10}(OH)_2 + H_2O = KAlSi_3O_8 + Al_2O_3 + \text{Melt} \quad (n)$$
muscovite K feldspar corundum

Phase assemblage on left-hand side of equilibrium is stable at low temperature relative to assemblage on right.

is greater than along Path 1 by a factor of about two. Melting in the model system in the presence of aluminosilicate and H_2O occurs at >2 GPa because of the lower temperature intersection of Path 2 and equilibrium *m*. Path 3 is characterized by such low temperatures to 2 GPa that water-rich aluminous minerals (kaolinite and diaspore) are stable to great depths, and melting in the model system will not occur. As noted above, an analysis allowing for compositional and structural variations in white micas and silica polymorphs would include stability fields for illite and amorphous silica at shallow levels along all paths; these would be limited to temperatures of less than ~200°C.

In general, the change in thermal regime from Path 1 to Path 3 makes the path of the slab-mantle interface similar to the Clapeyron slopes of dehydration equilibria (e.g., *e-h*, Table 1). This means H_2O may be stored in sediments to greater depths along cooler *PT* paths [*Peacock*, 1990, 1993]. Since H_2O is the principal solvent for material transport, this will result in metasomatic reactions proceeding at substantially greater depths when physical conditions favor cool *PT* paths. However, mineral solubilities generally decrease with decreasing temperature at constant pressure, so the extent of metasomatism may be low.

4. PHASE RELATIONS AS A FUNCTION OF DISSOLVED SILICA CONTENT

The concentration of aqueous silica ($SiO_{2(aq)}$) in H_2O in equilibrium with quartz has been determined experimentally by *Manning* [1994] at 0.5-2.0 GPa and 500-900°C. These experiments, combined with previous work, allow calculation of the concentration of $SiO_{2(aq)}$ in equilibrium with quartz from 25°C, 1 bar to >2 GPa and ~1000°C. Predicted $SiO_{2(aq)}$ molality ($m_{SiO_{2(aq)}}$) at quartz saturation are shown as a function of pressure and temperature in Figure 2b with the three *PT* paths. Below ~0.6 GPa and at high temperature, $m_{SiO_{2(aq)}}$ is sensitive to small changes in pressure at constant temperature because of correspondingly large changes in the density of H_2O with pressure. Above 1 GPa, isopleths of $SiO_{2(aq)}$ concentration have steep negative slopes. This indicates that high-temperature paths, which traverse isopleths at a high angle, will result in larger changes in quartz-saturated $SiO_{2(aq)}$ concentration along the slab than low-temperature paths.

By computing $m_{SiO_{2(aq)}}$ along Paths 1-3, the Si concentrations required by specific mineral assemblages may be determined, even if they do not include quartz. The concentration of $SiO_{2(aq)}$ in equilibrium with quartz (Figure 2b) can be used to constrain such an analysis because equilibrium between pure quartz and aqueous silica,

$$SiO_2 = SiO_{2(aq)} \quad (1)$$
quartz

requires at constant pressure and temperature that

$$\Delta G^\circ_{SiO_{2(aq)}} = \Delta G^\circ_{quartz} - RT \ln a_{SiO_{2(aq)}} \quad (2)$$

where ΔG° is the standard molal Gibbs free energy differ-

ence between a reference state (25°C, 10^5 Pa) and the P and T of interest, R is the gas constant, a is activity. In this study, standard states for minerals and water are unit activities of the pure phases at any pressure and temperature. Thermodynamic properties of the aqueous solution are taken to be those of pure H_2O.

The activity of $SiO_{2(aq)}$ can be equated to its molality because Si forms a neutral hydrated species with an activity coefficient of one over a wide range in pH [*Walther and Helgeson*, 1977]. Equation (2) thus becomes

$$\Delta G^\circ_{SiO_{2(aq)}} = \Delta G^\circ_{quartz} - RT \ln m_{SiO_{2(aq)}} \qquad (3)$$

which allows calculation of the standard molal Gibbs free energy of aqueous silica at the P and T of interest from ΔG°_{quartz} and $m_{SiO_{2(aq)}}$ as given by experiments and compilations of thermodynamic data. The value of $\Delta G^\circ_{SiO_{2(aq)}}$ may then be combined with thermodynamic data for minerals and H_2O to determine metasomatic phase relations as a function of silica concentration in the fluid. For example, the equilibrium between kaolinite and pyrophyllite at a given P and T,

$$\underset{\text{kaolinite}}{Al_2Si_2O_5(OH)_4} + 2SiO_{2(aq)} = \underset{\text{pyrophyllite}}{Al_2Si_4O_{10}(OH)_2} + H_2O \qquad (4)$$

leads to

$$\ln m_{SiO_{2(aq)}} = (\Delta_r G^\circ_{(4)})/2RT = (\Delta G^\circ_{py} + \Delta G^\circ_{H_2O} - \Delta G^\circ_{ka} - 2\Delta G^\circ_{SiO_{2(aq)}})/2RT \qquad (5)$$

where $\Delta_r G^\circ_{(4)}$ is the difference between standard molal Gibbs free energies of reactants and products for equilibrium (4).

Figure 3 shows calculated phase relations along Paths 1-3 assuming the presence of an Al- or Al-Si-bearing mineral. These phase diagrams differ from conventional diagrams describing Si metasomatism [e.g., *Hemley et al.*, 1980] in that pressure and temperature covary along the ordinate. The diagrams illustrate stability boundaries among both K-bearing phases (heavy lines) and K-absent phases (light lines). Thus, fields in Figure 3 represent the range of pressure, temperature, and fluid composition over which a K-bearing and a K-absent phase coexist with aqueous solution of varying Si concentration. Fields in Figure 3 are divariant, because pressure and temperature are not independent, and the system has four components. Similarly, phase boundaries represent the addition of a phase to the assemblage, and are therefore univariant. Fluids coexisting at equilibrium with three additional phases must adjust their composition as pressure and temperature change, if they are to remain on the phase boundary. Finally, four phases coexist with aqueous solution at phase-boundary intersections, which are invariant: any change in pressure, temperature, or fluid composition requires loss of one phase from the assemblage.

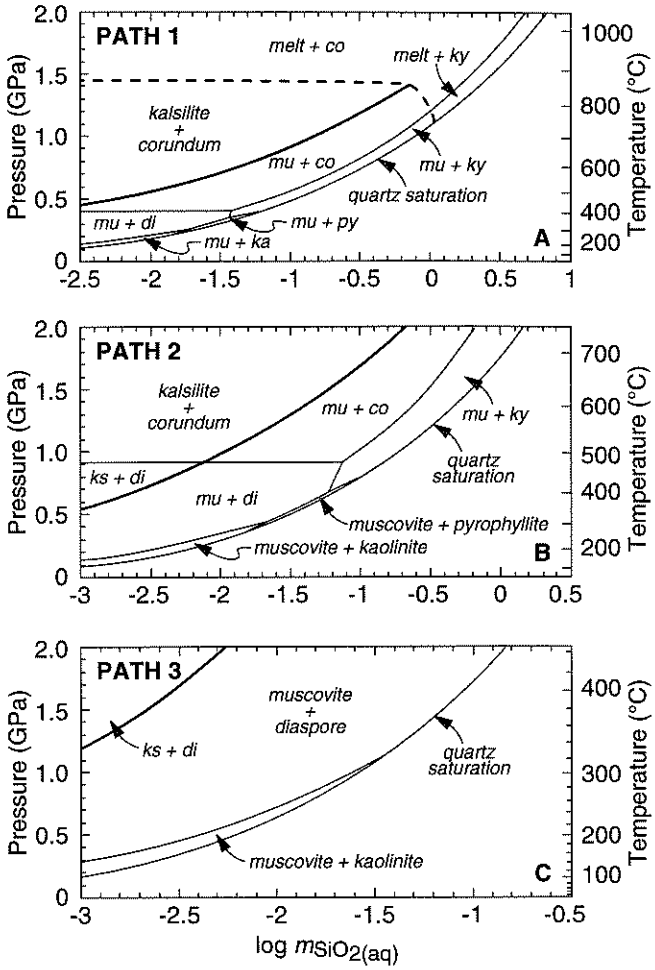

Fig. 3. Phase relations in the system K_2O-Al_2O_3-SiO_2-H_2O as a function of $SiO_{2(aq)}$ concentration and PT path. Light lines represent phase boundaries between stable minerals in the subsystem Al_2O_3-SiO_2-H_2O; heavy lines represent phase boundaries between stable K-bearing phases. The phase boundary involving KASH melt (heavy dashed line) is inferred from *Huang and Wyllie* [Figure 3, 1974]. Abbreviations as in Figure 3, except: mu, muscovite; py, pyrophyllite.

Melting in the KASH system occurs along Path 1 at <2 GPa (Figure 2a). The stability of a KASH melt as a func-

tion of $SiO_{2(aq)}$ concentration along Path 1 is shown schematically in Figure 3a. Si-rich bulk compositions containing quartz have the lowest solidus temperature in this system (reactions *m* and *n*, Figure 2a). Melting will therefore occur at the shallowest levels of warm subduction zones where aqueous fluids contain high dissolved silica contents (Figure 3). The depth of melting increases as $m_{SiO_{2(aq)}}$ decreases, and the total melting interval defined by variations in $m_{SiO_{2(aq)}}$ corresponds to a depth range of ~10 km, or 29 km of slab length. Note that, unlike minerals in Figure 3, the KASH liquid has variable composition.

Figure 3 represents a set of chemical maps that show how phase assemblage and fluid composition must change in model metasediments at the slab-mantle interface for different subduction scenarios. Along each path, the maximum molality of $SiO_{2(aq)}$ is defined by quartz saturation. Any metasediment containing quartz must lie on the phase boundaries labeled "quartz saturation," along which muscovite or KASH melt coexist with quartz and a K-absent, Al-bearing mineral at equilibrium (Figure 3). Fluids with greater Si contents are metastably supersaturated with respect to quartz, and must precipitate sufficient quartz to decrease $m_{SiO_{2(aq)}}$ until they lie on the quartz-saturation boundary. Fluids with $m_{SiO_{2(aq)}}$ below quartz saturation can not coexist with quartz at equilibrium. These fluids will be in equilibrium with quartz-absent phase assemblages, such as muscovite + corundum, or kalsilite + diaspore. Note that Figure 3 illustrates the well-known incompatibility certain mineral assemblages at equilibrium; for example, the Si-poor phases kalsilite or corundum will never be in equilibrium with quartz under the conditions considered, as they will react with quartz to form intervening muscovite or kyanite instead.

For any bulk composition, $m_{SiO_{2(aq)}}$ in coexisting fluid increases strongly with increasing depth (and correspondingly, temperature) along each subduction path. For example, $m_{SiO_{2(aq)}}$ in equilibrium with quartz-bearing assemblages along Path 3 will increase by a factor of ~10^3 (10^{-4} to >10^{-1} mol kg H_2O^{-1}) between 0 and 70 km; along Path 1, an even greater increase of ~10^5 times will occur (Figure 3). Below quartz saturation, all univariant phase boundaries buffer $m_{SiO_{2(aq)}}$ along the slab-mantle interface, and their positive slopes indicate that they similarly require increasing $m_{SiO_{2(aq)}}$ with depth for quartz-absent assemblages.

Figure 3 shows that the presence of two or more Si-bearing minerals in the KASH system requires $SiO_{2(aq)}$ concentrations within several tenths of a log unit of quartz saturation. This implies that at a given pressure and temperature, the absence of quartz, or its loss through dissolution, will result in only minor changes in $SiO_{2(aq)}$ concentration compared to those attending variation in pressure and temperature. Si mass transfer in sediments in subduction zones can therefore be reasonably assumed to occur at, or very close to, quartz saturation, which means that $m_{SiO_{2(aq)}}$ will be maximized in the presence of sediment. The rarity of silica undersaturated phases, like corundum and kalsilite, in exposed metasediments from subduction-zone settings supports this conclusion.

5. IMPLICATIONS

Phase relations among model KASH sediment and aqueous fluid (Figure 3) illustrate three important points about material transport and metasomatism in subduction zones. The first is that, for Si redistribution, the dissolved silica content of pore fluids in metasediments, and its change as subduction proceeds, depends strongly on the *PT* path followed by the subduction zone. As shown in Figure 3, $m_{SiO_{2(aq)}}$ in equilibrium with quartz-bearing assemblages increases with temperature. This indicates that conditions which lead to high temperatures in subduction zones (e.g., young oceanic crust, incipient subduction, high shear stress, low slab velocities) maximize the potential for aqueous transport of silica. A particularly well-documented natural example illustrating this observation is described by *Bebout and Barton* [1993] on Santa Catalina Island, California.

The second implication of Figure 3 is that increases in $SiO_{2(aq)}$ must be achieved by dissolving silica from coexisting minerals. Thus, as model KASH metasediments are subducted along different PT paths, their bulk compositions will become progressively depleted in Si with depth in the presence of a static pore fluid. Like the amount of dissolved silica, the magnitude of the shift in bulk composition will be greater for higher temperature paths. In addition, if metasediment is returned to the surface, dissolved silica in static pore fluids must decrease, leading to precipitation of silica-rich phases such as quartz.

Finally, along with lithologically controlled bulk compositional differences, the changes in dissolved silica with path and depth represent the driving potential for Si metasomatism by flowing fluid (Figure 1). As pore fluids migrate independently of the rock matrix in a model KASH metasediment, their compositions must adjust at equilibrium as required by the relevant phase relations [e.g., Figure 3]. This will lead to shifts in bulk composition of varying magnitude in the rocks through which the fluid flows. For fluids migrating from the slab-mantle interface into the mantle wedge, the presence of sediment will maximize the amount of dissolved silica redistributed form slab to mantle, regardless of the depth at which the fluids leave the slab [see *Manning*, 1995].

Fluids may also migrate updip along the slab-mantle interface. The potential for Si transfer back up the slab along a sediment veneer can be assessed by evaluating the change in $m_{SiO2(aq)}$ at quartz saturation along each path. Figure 4a shows the quantity $dm_{SiO2(aq)}/dz$, where z is distance in kilometers along the subducting slab for Paths 1-3. This quantity was obtained from finite difference derivatives of quartz solubility as a function of pressure (Figure 3), with pressure transformed to distance using a rock density of 3000 kg m^{-3} and a 20° slab angle. The change in quartz solubility with position in the slab is greater for higher temperature paths, just as absolute solubilities are higher along higher temperature paths (Figure 2b). Because the change in solubility will require quartz precipitation or dissolution at equilibrium, higher temperature paths have a significantly greater capacity to redistribute Si than cooler paths.

The magnitude of this difference can be appreciated by integrating $dm_{SiO2(aq)}/dz$ over the length of the flow path along the slab. For example, assuming that quartz-saturated H_2O begins migrating updip in sediments at a depth corresponding to 185 km along the slab surface, and that this fluid remains in equilibrium with quartz along its flow path, the volume of quartz precipitated during upward flow to the Earth's surface will be ~0.4 cm^3 kg H_2O^{-1}, ~0.1 cm^3 kg H_2O^{-1}, and ~0.01 cm^3 kg H_2O^{-1} along Paths 1, 2, and 3, respectively (Figure 4b). In addition, most of the increase in the amount of quartz precipitated occurs in the deep parts of the slab. Veins of quartz, which are common in subducted metasediments [e.g., *Bebout and Barton*, 1989; *Ernst*, 1990], require removal of Si from the fluid in response to solubility decreases along its flow path. Figure 4 implies that for constant flux, the greatest volume of vein quartz should be expected to originate in the deeper parts of any given subduction zone, and that high-temperature paths will result in larger volumes of precipitated quartz.

In conclusion, this analysis shows that because most flux trajectories carry aqueous fluids through sediment at the slab-mantle interface (Figure 1), chemical interaction between sediment and fluid must be taken into account in considering aqueous mass transfer. For Si, it is likely that sediment-fluid interaction will result in high $SiO_{2(aq)}$ concentrations, at or near quartz saturation. If this fluid migrates back up the slab, the decrease in quartz solubility with pressure and temperature will lead to precipitation of quartz in fluid conduits such as fractures. If the fluid migrates into the low-Si environment of the mantle-wedge, the result may be substantial increases in the mantle SiO_2 content near the slab through conversion of olivine and orthopyroxene to, for example, talc and Fe-Mg amphibole [e.g., *Bebout and Barton*, 1993; *Manning*, 1995].

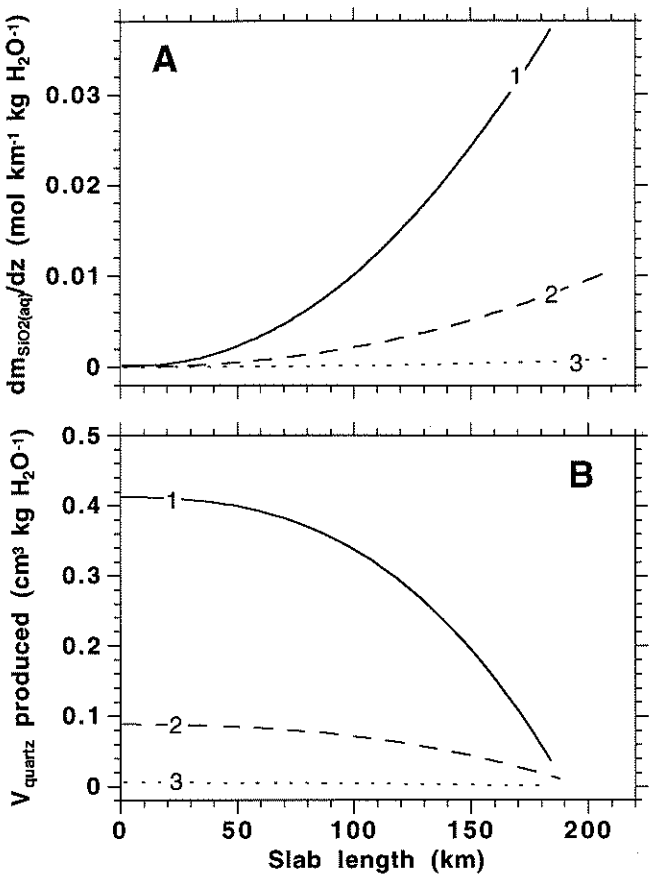

Fig. 4. (A) Change in concentration of aqueous silica in equilibrium with quartz ($dm_{SiO2(aq)}/dz$) with distance along slab for different PT paths (1-3). (B) Volume of quartz produced by quartz-saturated H_2O migrating updip along Paths 1-3 185 km from the trench.

Acknowledgments. This study was funded by NSF EAR-9405999. Thanks to M. Barton, G. Nichols, and P. Vrolijk for insightful reviews. M Grove, K. Knesel, and D. Rothstein read and improved an early draft of the manuscript.

REFERENCES

Ayers, J. C., and E. B. Watson, Solubility of apatite, monazite, zircon, and rutile in supercritical fluids with implications for subduction zone geochemistry, *Philos. Trans. R. Soc. London, Ser. A, 335*, 365-375, 1991.

Ayers, J. C., and E. B. Watson, Rutile solubility and mobility in supercritical aqueous fluids, *Contrib. Mineral. Petrol., 114*, 321-330, 1993.

Bebout, G. E., Geometry and mechanisms of fluid flow at 15 to 45 kilometer depths in an Early Cretaceous accretionary complex, *Geophys. Res. Lett., 18*, 923-926, 1991.

Bebout, G. E., and M. D. Barton, Fluid flow and metasomatism in a subduction zone hydrothermal system: Catalina Schist terrane, California, *Geology, 17*, 976-980, 1989.

Bebout, G. E., and M. D. Barton, Metasomatism during subduction: Products and possible paths in the Catalina Schist, California, *Chem. Geol., 108*, 61-92, 1993.

Berman, R. G., Internally-consistent thermodynamic data for minerals in the system Na_2O-K_2O-CaO-MgO-FeO-Fe_2O_3-Al_2O_3-SiO_2-TiO_2-H_2O-CO_2, *J. Petrol., 29*, 445-522, 1988.

Brenan, J. M., 1993, Partitioning of fluorine and chlorine between apatite and aqueous fluids at high pressure and temperature: implications for the F and Cl content of high P-T fluids, *Earth Planet. Sci. Lett., 117*, 251-263, 1993.

Brenan, J. M., and E. B. Watson, Partitioning of trace elements between olivine and aqueous fluids at high P-T conditions: Implications for the effect of fluid composition on trace element transport, *Earth Planet. Sci. Lett., 107*, 672-688, 1991.

Church, S. E., The Cascade mountains revisited: a re-evaluation in light of new lead isotopic data: *Earth Planet. Sci. Lett., 29*, 175-188, 1976.

Davies, J. H., and D. J. Stevenson, Physical model of source region of subduction zone volcanics, *J. Geophys. Res., 97*, 2037-2070, 1992.

Ernst, W. G., Thermobarometric and fluid expulsion history of subduction zones, *J. Geophys. Res., 95*, 9047-9053, 1990.

Haar, L., J. S. Gallagher, and G. S. Kell, *NBS/NRC Steam Tables*, 320 pp., Hemisphere, New York, NY, 1984.

Hemley, J. J., J. W. Montoya, J. W. Marinenko, and R. W. Luce, Equilibria in the system Al_2O_3-SiO_2-H_2O and some general implications for alteration/mineralization processes, *Econ. Geol., 75*, 210-228, 1980.

Huang, W. L., and P. J. Wyllie, Melting relations of muscovite with quartz and sanidine in the K_2O-Al_2O_3-SiO_2-H_2O system to 30 kilobars and an outline of paragonite melting relations, *Am. J. Sci., 274*, 378-395, 1974.

Kay, R. W., S.-S. Sun, and S.-N. Lee-Hu, Pb and Sr isotopes in volcanic rocks from the Aleutian Islands and Pribilof Islands, Alaska, *Geochim. Cosmochim. Acta, 42*, 263-273, 1978.

Kyte, F. T., M. Leinen, G. R. Heath, and L. Zhou, Cenozoic sedimentation history of the central North Pacific: inferences from the elemental geochemistry of core LL44-GPC3. *Geochim. Cosmochim. Acta, 57*, 1719-1740, 1993.

Manning, C. E., The solubility of quartz in the lower crust and upper mantle, *Geochim. Cosmochim. Acta, 58*, 4831-4839, 1994.

Manning, C. E., Coupled reaction and flow in subduction zones: Si metasomatism in the mantle wedge, in *Fluid Flow and Transport in Rocks*, edited by B. Jamtveit and B. W. D. Yardley, Chapman and Hall, in press, 1995.

Manning, C. E., and S. L. Boettcher, Rapid-quench hydrothermal experiments at mantle pressures and temperatures, *Am. Mineral., 79*, 1153-1158, 1994

Moore, J. C., Selective subduction, *Geology, 3*, 530-532, 1975.

Morris, J. D., W. P. Leeman, and F. Tera, The subducted component in island arc lavas: Constraints from Be isotopes and B-Be systematics, *Nature, 344*, 31-36, 1990.

Nichols, G. T., P. J. Wyllie, and C. R. Stern, Subduction zone melting of pelagic sediments constrained by melting experiments, *Nature, 371*, 785-788, 1994.

Peacock, S. M., Fluid processes in subduction zones, *Science, 248*, 329-337, 1990.

Peacock, S. M., The importance of blueschist → eclogite dehydration reactions in subducting oceanic slabs, *Geol. Soc. Am. Bull., 105*, 684-694, 1993.

Peacock, S. M., T. Rushmer, and A. B. Thompson, Partial melting of subducting oceanic crust, *Earth Planet. Sci. Letters, 121*, 227-244, 1994.

Philippot, P., Fluid-melt-rock interaction in mafic eclogites and coesite-bearing metasediments: constraints on volatile recycling during subduction, *Chem. Geol., 108*, 93-112, 1993.

Plank, T., Mantle melting and crustal recycling in subduction zones, Ph.D. Thesis, 444 pp., Columbia University, New York, 1993.

Plank, T., and J. N. Ludden, Geochemistry of sediments in the Argo abyssal plain at Site 765: a continental margin reference section for sediment recycling in subduction zones, *Proc. Ocean Drill. Program: Sci. Results, 123*, 167-189, 1992.

Plank, T., and C. H. Langmuir, Tracing trace elements from sediment input to volcanic output at subduction zones, *Nature, 362*, 739-743, 1993.

Storre, B., and E. Karotke, Experimental data on melting reactions of muscovite + quartz in the system K_2O-Al_2O_3-SiO_2-H_2O to 20 Kb water pressure, *Contrib. Mineral. Petrol., 36*, 343-345, 1972.

Sun, S.-S., Lead isotopic study of young volcanic rocks from mid-ocean ridges, ocean islands and island arcs: *Philos. Trans. R. Soc. London, Ser. A, 297*, 409-445, 1980.

Tatsumi, Y., Migration of fluid phases and genesis of basalt magmas in subduction zones, *J. Geophys. Res., 94*, 4697-4707, 1989.

Tera, F., L. Brown, J. Morris, I. S. Sacks, J. Klein, and R. Middleton, Sediment incorporation in island-arc magmas: Inferences from ^{10}Be, *Geochim. Cosmochim. Acta, 50*, 535-550, 1986.

von Heune, R., and D. W. Scholl, Observations at convergent margins concerning sediment subduction, subduction erosion, and the growth of continental crust, *Rev. Geophys., 29*, 279-316, 1991.

Walther, J. V., and H. C. Helgeson, Calculation of the thermodynamic properties of aqueous silica and the solubility of quartz and its polymorphs at high pressures and temperatures, *Am. J. Sci., 277*, 1315-1351, 1977.

White, W. M., and B. Dupré, Sediment subduction and magma genesis in the Lesser Antilles: Isotopic and trace element constraints, *J. Geophys. Res., 91*, 5927-5941, 1986.

Whitford, D. J., and P. A. Jezek, Isotopic constraints on the role of subducted sialic material in Indonesian island-arc magmatism. *Geol. Soc. Am. Bull., 93*, 504-513, 1982.

C. E. Manning, Department of Earth and Space Sciences, University of California, Los Angeles, CA, 90024-1567.